Journal of Nanobiotechnology

RESEARCH

Open Access

Multifunctional hydrogel targeting senescence to accelerate diabetic wound healing through promoting angiogenesis

Hao Yang[1†], Yongfei Chen[1†], Yanchao Rong[1†], Yuxi Zhou[1†], Shuting Li[2†], Xiaohui Li[1], Honglin Wu[1], Dongming Lv[1], Xiaoling Cao[1], Peng Wang[1], Jiayuan Zhu[1*], Bing Tang[1*] and Zhicheng Hu[1*]

Abstract

Diabetic wound healing remains a significant clinical challenge because of hyperglycaemia-induced cellular senescence, impaired angiogenesis, and chronic inflammation. To address these issues, we developed a multifunctional hydrogel (GelMA/PNS/Alg@IGF-1) that integrates gelatine methacryloyl (GelMA), Panax notoginseng saponins (PNS), and sodium alginate microspheres encapsulating insulin-like growth factor-1 (IGF-1). This hydrogel was engineered to achieve gradient and sustained release of bioactive agents to target senescence and promote vascular repair. In vitro studies demonstrated that the hydrogel significantly reduced oxidative stress, suppressed senescence markers and senescence-associated secretory phenotypes, and restored endothelial cell function under high-glucose conditions by inhibiting NF-κB pathway activation. Transcriptomic analysis revealed the modulation of pathways linked to inflammation, apoptosis, and angiogenesis. This hydrogel accelerated diabetic wound closure in a rat model in vivo and enhanced collagen deposition, granulation tissue formation, and neovascularization. Furthermore, the hydrogel mitigated oxidative stress and cellular senescence and promoted tissue remodelling. The synergistic effects of PNS and IGF-1 within the hydrogel established a pro-regenerative microenvironment to address both pathological ageing and vascular dysfunction. These findings highlight GelMA/PNS/Alg@IGF-1 as a promising therapeutic platform for diabetic wound management, as this material offers dual anti-senescence and proangiogenic efficacy to overcome the complexities of chronic wound healing.

†Hao Yang, Yongfei Chen, Yanchao Rong, Yuxi Zhou and Shuting Li contributed equally to this work.

*Correspondence:
Jiayuan Zhu
zhujiay@mail.sysu.edu.cn
Bing Tang
tangbing@mail.sysu.edu.cn
Zhicheng Hu
huzhch5@mail.sysu.edu.cn

Full list of author information is available at the end of the article

Graphical abstract

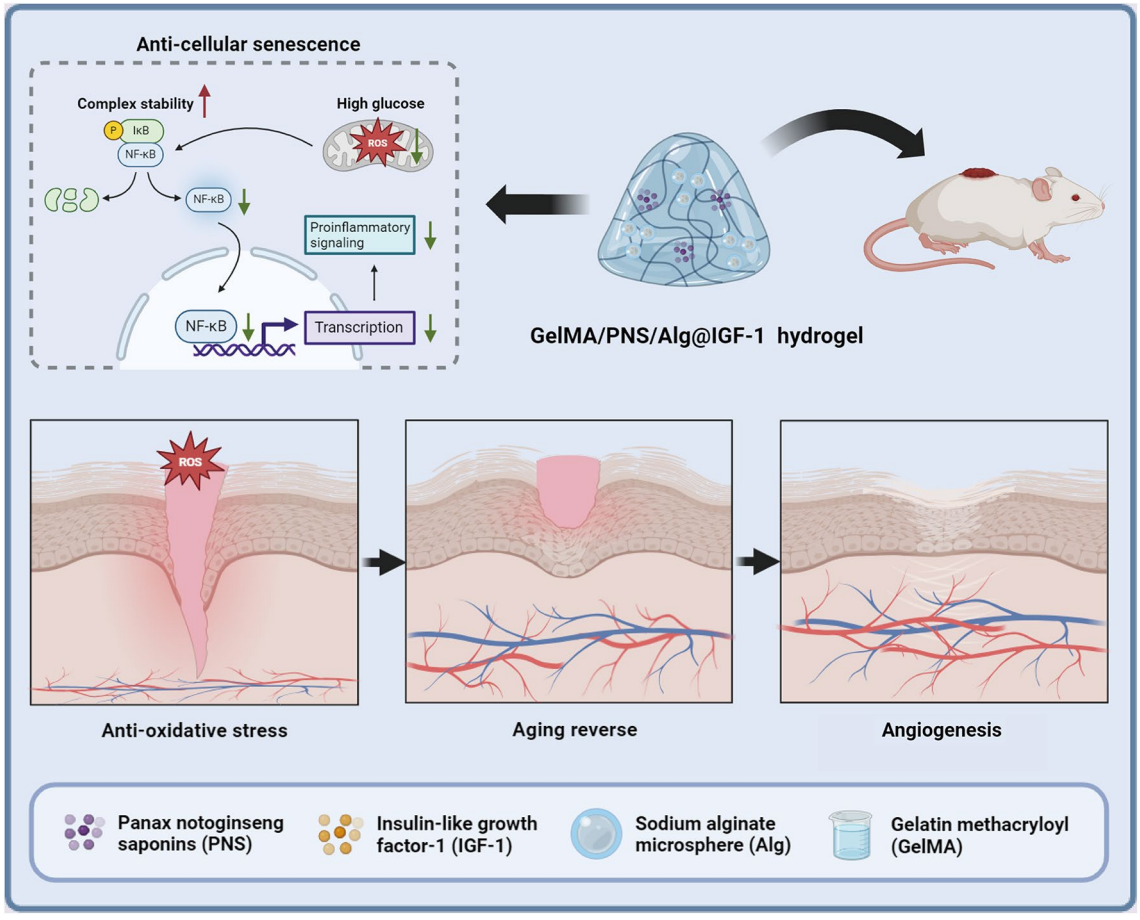

Keywords Diabetic wound healing, Panax Notoginseng saponins, Insulin-like growth factor-1, Gelatine methacryloyl hydrogel, Sodium alginate microspheres

Introduction

Chronic diabetic wounds pose a significant global health challenge and are characterized by delayed healing, persistent inflammation, and impaired vascularization, which result from the pathological effects of hyperglycaemia [1]. These wounds severely compromise patients' quality of life and place a heavy financial burden on health care systems. Impaired angiogenesis, driven by endothelial dysfunction, oxidative stress, and cellular senescence, represents one of the primary barriers to effective diabetic wound healing [2, 3]. Cellular senescence, a state of irreversible cell cycle arrest, is particularly exacerbated in the high-glucose environment of diabetic wounds, where it promotes chronic inflammation, inhibits angiogenesis, and delays tissue repair [4, 5]. Consequently, targeting cellular senescence and promoting angiogenesis are essential strategies for the development of effective therapies for diabetic wound management.

Hydrogels have emerged as promising platforms for wound healing because of their ability to create a moist wound environment, deliver bioactive agents, and mimic the extracellular matrix (ECM) [6, 7]. Among these, multifunctional hydrogels that integrate biomaterials with therapeutic agents hold immense potential for addressing the complex pathophysiology of diabetic wounds. Gelatine methacryloyl (GelMA)-based hydrogels, in particular, have gained attention for their excellent biocompatibility, tunable mechanical properties, and capacity to support cell adhesion, proliferation, and migration [8, 9]. When combined with bioactive molecules, GelMA hydrogels can be engineered to enable sustained drug delivery and exert synergistic effects, enhancing the wound healing process.

Panax notoginseng saponins (PNS), a group of natural compounds extracted from Panax notoginseng, possesses potent antioxidant, anti-inflammatory, and

proangiogenic properties, and thus it is a promising candidate for promoting vascularization and tissue repair [10, 11]. Similarly, insulin-like growth factor-1 (IGF-1), a crucial member of a multifunctional growth factor family, plays a pivotal role in tissue repair by mediating angiogenesis, cellular proliferation, and tissue remodelling [12–14]. However, the clinical application of PNS and IGF-1 is hindered by their instability, short half-life, and rapid degradation in the wound environment, which significantly limits their therapeutic potential [15–17]. To address these challenges, the encapsulation of bioactive agents within hydrogels offers an effective controlled delivery system that protects their bioactivity, ensures sustained release, and optimizes therapeutic efficacy [18].

An orderly and appropriate drug gradient release is crucial for effective wound healing [19]. The sequential release of anti-inflammatory agents, proangiogenic drugs, and growth factors aligns with the dynamic phases of diabetic wound healing [20]. However, limitations such as the short half-life, low bioavailability, and differential release profiles of therapeutic agents necessitate the development of advanced drug delivery systems [21]. Among various carriers, microspheres are particularly attractive because of their unique spherical polymeric network, which provides a large surface area-to-volume ratio and spatiotemporal control over drug release, thereby enhancing the efficacy of encapsulated agents [22, 23]. The integration of microspheres into hydrogels can further optimize drug delivery and provides a multifunctional platform for sequential and sustained therapeutic release.

In this study, we developed a novel multifunctional GelMA hydrogel loaded with PNS and sodium alginate microspheres encapsulating IGF-1 (GelMA/PNS/Alg@IGF-1). This hydrogel was designed to target cellular senescence and promote angiogenesis in diabetic wounds (Fig. 1). The dual-barrier delivery system of the GelMA hydrogel and microspheres enabled both gradient and sequential release of PNS and IGF-1, which addresses the requirements of different stages of wound healing. Comprehensive in vitro and in vivo evaluations of its physicochemical properties, biocompatibility, and therapeutic efficacy were performed. The results demonstrated that the GelMA/PNS/Alg@IGF-1 hydrogel possesses excellent stability, controlled release properties, and the ability to alleviate oxidative stress, suppress cellular senescence, and enhance angiogenesis. The multifunctional GelMA/PNS/Alg@IGF-1 hydrogel holds great potential as an advanced wound dressing and could provide an effective solution for the treatment of this complex medical challenge.

Materials and methods

Reagents and materials

Gelatine (Gel), methacrylic anhydride (MA), sodium alginate (Alg), PNS, and anhydrous calcium chloride were purchased from Macklin Biochemical Co., Ltd. (Shanghai, China). IGF-1 (712104) was purchased from BioLegend, Inc. (San Diego, USA). Irgacure 2959 was purchased from Yinchang New Materials Co., Ltd. (Shanghai, China). Phosphate-buffered saline (PBS) was purchased from Dingguo Changsheng Biotechnology Co., Ltd. (Beijing, China). Streptomycin sulfate, foetal calf serum, trypsin, penicillin, EDTA, and CCK-8 were purchased from Beinuo Biotechnology Co., Ltd. (Shanghai, China). Lysozyme was obtained from Yuanye Bio-Technology Co., Ltd. (Shanghai, China). All other chemicals were of analytical reagent grade and were used without further processing.

GelMA synthesis

GelMA was synthesized according to a previous report [24], with some modifications. Briefly, 10 g of gelatine was dissolved in 100 mL of distilled water, after which 15 mL of methacrylic anhydride was added to the gelatine mixture. The mixture was allowed to react at 50 °C for 4 h. The resulting mixture was then dialyzed (molecular weight cut-off: 10 kDa) for 2–3 days and lyophilized at -80 °C.

Synthesis of Alg@IGF-1 microspheres

Alg@IGF-1 microspheres were synthesized according to a previous report [25]. A 2 wt% sodium alginate solution was prepared (aqueous phase). IGF-1 was then added to the alginate solution at a mass ratio of 10^{-5} and stirred uniformly for subsequent use. The organic phase was prepared by mixing 1%wt Tween-80 into olive oil with mechanical stirring at 600–750 rpm for 1–2 h. Next, 20 mL of the aqueous phase was added to 100 mL of the organic phase with mechanical stirring at 650–700 rpm; the mixture was then stirred at 750 rpm for 1 h. Subsequently, 40 mL of 96% calcium chloride solution was added to the mixture with stirring at 500 rpm for 1 h. Next, 10 mL of isopropyl ketone was added to this mixture with mechanical stirring at 400 rpm for 30 min. The mixture was then centrifuged at 6000 rpm for 5–10 min, and the sediment was washed and centrifuged alternately with distilled water and isopropyl ketone 23 times at 6000 rpm for 5–10 min. Finally, the sediment was freeze-dried to obtain IGF-1-coated sodium alginate microspheres (Alg@IGF-1).

Preparation of the GelMA/PNS/Alg@IGF-1 hydrogel

Four groups of hydrogel samples were obtained by mixing GelMA, PNS, and Alg@IGF-1 at the concentrations presented in Supplementary Table 1. The GelMA hydrogel was obtained by mixing 10% (w/v) GelMA and 1% wt Irgacure 2959. This solution was then irradiated with UV light for 30 min to enable crosslinking of the hydrogel. A similar process was used to prepare the GelMA/

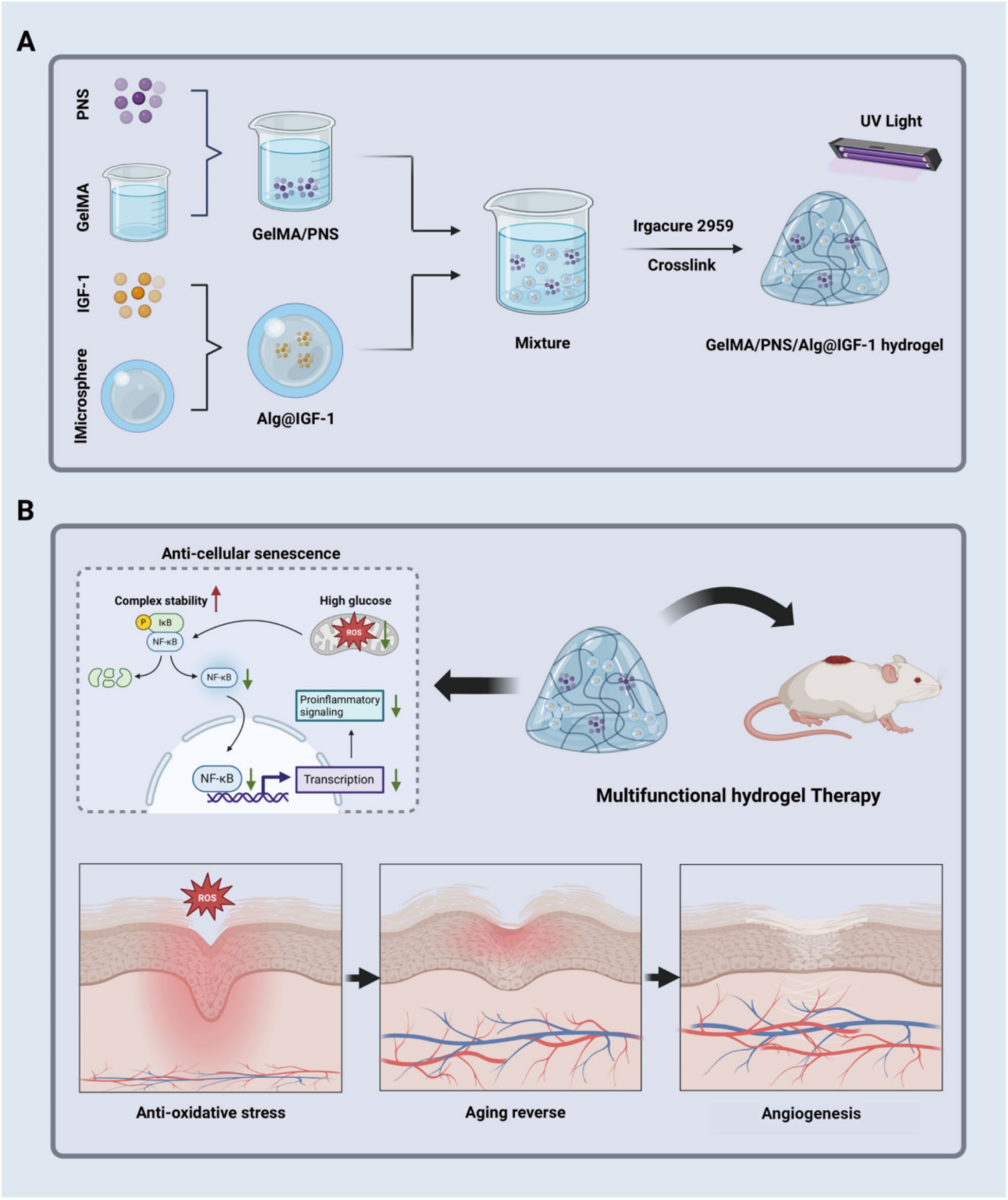

Fig. 1 Preparation of the multifunctional GelMA/PNS/Alg@IGF-1 hydrogel (**A**) and the intricate mechanism through which it facilitates diabetic wound healing (**B**)

PNS, GelMA/Alg@IGF-1, and GelMA/PNS/Alg@IGF-1 hydrogels.

Characterization

A nuclear magnetic resonance (NMR) spectrometer (Bruker AV-500; Bruker, Germany) was used to investigate the nuclear magnetic properties of the hydrogel. Fourier transform infrared (FTIR) spectra of the hydrogel components were acquired via an FTIR spectrometer (Vertex 70; Bruker). Scanning electron microscopy (SEM, S-3400; Hitachi, Japan) was used to assess the micromorphology of the microspheres and hydrogel. A material testing machine (ElectroForce 3220, Bose, USA) was used to determine the compression properties of the hydrogel.

Swelling properties

The swelling property of the hydrogel was tested by placing the hydrogel on wet filter paper. The initial weight (W_{s0}) and swelling weight (W_s) of the hydrogel at different time intervals were recorded, and the swelling ratio was calculated using the following equation: swelling ratio = $(W_s - W_{s0})/W_{s0}$ [26].

In vitro degradation

The hydrogel was freeze-dried and immersed in a lysozyme solution (1000 U/mL in PBS, pH 7.4). All samples were placed in a constant-temperature shaker (37 °C, 70 rpm) and weighed at different time intervals. The initial weight and final weight of the remaining hydrogel after degradation were recorded as W_{d0} and W_d, respectively. The degradation ratio was calculated using the following equation: degradation ratio (%) = $(W_d/W_{d0}) \times 100\%$ [26].

In vitro release of PNS and IGF-1

The in vitro release of PNS was determined on the basis of the cumulative release rate. High-performance liquid chromatography (HPLC 15235, Waters, USA) was used to determine the release rate of PNS. An IGF-1 ELISA kit (Magellan, Switzerland) was used to determine the entrapment efficiency and in vitro release rate of IGF-1.

Cell culture

HUVECs (human umbilical vein endothelial cells) and NHDFs (normal human dermal fibroblasts) were purchased from the Cell Bank of Typical Culture Preservation Committee of the Chinese Academy of Sciences. The cells were maintained at 37 °C in a humidified atmosphere with 5% CO_2, and the culture medium was replaced every 48 h. HUVECs were seeded into 6-well plates at a density of 3×10^6 cells per well. The GelMA, GelMA/PNS, GelMA/Alg@IGF-1, and GelMA/PNS/Alg@IGF-1 hydrogels were subsequently placed in the upper chamber of a Transwell plate, and the cells were cocultured for further experiments.

Cytocompatibility test

The hydrogel extract was prepared and stored at 4 °C until use. Fibroblasts, whose density was maintained at 10^5 cells/mL, were seeded in a 96-well plate (100 μL/well; experimental group [EG]). A blank control group (CG, 100 μL of culture media without cells) and a negative control group (NG, 100 μL of culture media with cells) were also prepared. The cells were cultured in growth medium at 37 °C in an atmosphere of 5% CO_2. Following the attachment of the cells to the well, the culture medium was replaced with 100 μL of leach liquor. At a predetermined time point, the leach liquor was removed, and 100 μL of fresh culture media containing 10 μL of CCK-8 reagent was added to each well, after which the cells were incubated for 4 h. The absorbance value was measured at 450 nm in a microplate reader (Magellan). All the tests were conducted in quintuplicate. The relative growth rate (RGR) was calculated according to the following equation: RGR (%) = $(OD_{EG} - OD_{CG})/OD_{NG} \times 100\%$.

Assessment of apoptosis

A Hoechst 33,342/propidium iodide (PI) Kit (Beyotime; China) was used to assess the number of apoptotic cells according to the manufacturer's instructions. Red and blue hyperfluorescence was observed in necrotic cells.

Cell migration assay

Cell migration ability was evaluated via a Transwell assay. To establish the coculture system, the GelMA, GelMA/PNS, GelMA/Alg@IGF-1, and GelMA/PNS/Alg@IGF-1 hydrogels were individually placed in the lower chamber of a 24-well Transwell plate (Corning, USA). The cell suspensions were diluted in serum-free medium and seeded into the upper chamber, while complete medium was added to the lower chamber. After 24 h of incubation, nonmigrated cells on the upper membrane were carefully removed. The migrated cells on the lower surface were fixed and stained with crystal violet (Beyotime, China). Following washing with PBS, the stained cells were quantified under a light microscope.

Tube formation assay

HUVECs (3×10^3 cells/well) were seeded into 96-well culture plates precoated with Matrigel™ Matrix Growth Factor Reduced (BD Biosciences, USA). After the cells were incubated at 37 °C for 6 h, an inverted phase contrast microscope (Leica Microsystems GmbH, Germany) was used to count the number of capillary network meshes in five random fields per culture plate well.

Transcriptome sequencing

After the treated cells were collected, TRIzol was used for cell lysis and total RNA extraction. The cDNA libraries were subjected to sequencing on the Illumina sequencing platform by Genedenovo Biotechnology Co. Ltd. (Guangzhou, China). DEGs were determined by an FDR < 0.05 and|log2FC|>1. A bioinformatic analysis was performed via OmicsMart, a real-time interactive online platform for data analysis (http://www.omicsmart.com).

Network pharmacological analysis

We utilized the Traditional Chinese Medicine Systems Pharmacology (TCMSP), HERB, and SwissTargetPrediction (STP) databases to identify potential therapeutic targets of PNS. Additionally, key targets related to diabetic wounds or diabetic ulcers were identified via the Online Mendelian Inheritance in Man (OMIM) database, GeneCards database, Disease Gene Network (DisGeNet) database, DRUGBANK database, and Therapeutic Target Database (TTD). Furthermore, the GeneMANIA database was used to visualize the interaction network of IGF-1. For gene set functional enrichment analysis, we used the R software package clusterProfiler (version 3.14.3) to obtain the results of the gene set enrichment.

Senescence-Associated β-Galactosidase (SA-β-gal) staining

In accordance with the protocol of the SA-β-gal Staining Kit (Beyotime; China), the cells were washed with PBS and incubated in stationary liquid for 15 min at room temperature. After three washes in PBS for 3 min each time, the cells were incubated in the staining working solution at 37 °C without CO_2 for 14 h. The following day, the staining working solution was discarded, and the cells were washed three times with PBS. Finally, the samples were examined under a microscope.

Detection of ROS

After they were washed with PBS, the treated cells were incubated with the DCFH-DA fluorescent probe (Beyotime; China) for 30 min at 37 °C. Once the incubation was complete, the cells were washed to remove any unbound probe. The ROS fluorescence intensity was then measured via fluorescence microscopy. Fresh wound tissue can be analysed via DHE staining.

Mitochondrial membrane potential (φM)

The lipophilic cationic dye JC-1 (MCE, USA), which is selectively taken up by mitochondria, was employed to visualize the mitochondrial membrane potential. JC-1 was added to the HUVEC culture at a final concentration of 2 μm, and after a 15-min incubation, changes in the mitochondrial membrane potential were evaluated by observing alterations in the fluorescence intensity of monomers and multimers via fluorescence microscopy.

Quantitative Real-Time polymerase chain reaction (qRT–PCR)

The expression levels of p21 and p53 were detected by qRT−PCR. RNA was extracted using a TRIzol kit (Life Technologies, USA), and first-strand cDNA was synthesized via reverse transcription using a gDNAEr Reagent Kit (Takara, Japan) according to the manufacturer's protocol. qRT−PCR was performed using a Bestar®SybrGreen qPCR Master Mix (DBI, Germany). The sequences of the primers used for qRT−PCR are shown in Supplementary Table 2.

Western blot

Proteins from cultured cells were extracted with RIPA lysis buffer (MIK, China). The total concentration of protein collected from the cells was calculated using a BCA protein assay kit (Solarbio, China). Protein samples were separated by SDS−PAGE and transferred to PVDF membranes (Millipore, USA). After the membranes were blocked, they were incubated overnight at 4 °C with primary antibodies against GAPDH (60004-1-Ig), NF-κB p65 (10745-1-AP), phospho-NF-κB p65 (80379-2-RR), IκBα (10268-1-AP), and phospho-IκBα (82349-1-RR). An HRP-labelled secondary antibody was used to detect the antibody reactivity. The protein signal was detected via chemiluminescence western blotting detection solution (Bio-Rad, USA).

Enzyme-linked immunosorbent assay (ELISA)

To detect the release of SASP factors (IL-1β and IL-6), ELISA was performed using a human ELISA kit (Meimian, China), and the absorbance at 450 nm was measured with a microplate reader within 15 min after the reaction was stopped.

In vivo diabetic wound healing test

All animal experimental procedures were approved by the Institutional Review Board of the First Affiliated Hospital of Sun Yat-Sen University. During the animal study, the rats were raised in a specific pathogen-free environment with an adequate supply of food and water. The rat model of diabetes was established according to a previous study [27]. Healthy female Sprague–Dawley rats weighing 250 g were intraperitoneally injected with streptozotocin (65 mg/kg). One week later, the rats with blood glucose levels greater than 16 mmol/L and other symptoms, i.e., polyphagia, polydipsia, polyuria, and weight loss, were considered successful type 1 diabetic model rats.

Before surgery, all rats were anaesthetized with pentobarbital sodium (30 mg/kg), and their dorsal hair was shaved. Two circular full-thickness skin wounds 2.0 cm in diameter were generated on the backs of each rat by excising the skin tissue with sterile dissecting scissors. All rats were randomly assigned to one of 4 groups, and their

wounds were covered with each of 4 different hydrogel dressings; the dressings were fixed in place with a surgical cord. All the rats were housed in individual cages after surgery. The wounds were observed on postoperative days 3, 7, 14, and 21.

Histologic analysis

Samples obtained at 7, 14, and 21 days after surgery were fixed in 4% paraformaldehyde for at least 24 h. The samples were then dehydrated in a graded series of ethanol and embedded in paraffin for haematoxylin–eosin (H&E) staining and Masson's trichrome staining. The stained sections were observed under an optical microscope.

Immunofluorescence staining

The paraffin sections were deparaffinized, cleared 3 times in xylene for 15 min, and then rehydrated in absolute ethanol two times for 5 min each time, one time each in 85% ethanol and 75% ethanol for 5 min, and finally, one time in distilled water. The slides were then incubated overnight at 4 °C with primary antibodies against α-smooth muscle actin (α-SMA) and CD31. After they were rinsed 3 times in PBS (pH 7.4) for 5 min, the slides were incubated with secondary antibodies at room temperature for 50 min. Subsequently, the slides were incubated with DAPI in the dark for 10 min after additional washes in PBS. The sections were observed with a confocal laser scanning microscope.

Immunohistochemistry (IHC)

The paraffin sections were deparaffinized and washed according to the method described above. The sections were blocked with 3% BSA blocking buffer for 30 min. The slides were then incubated overnight at 4 °C with primary antibodies against p16, IL-6, TGF-β1, TGF-β3, TNF-α, and CD31. After they were rinsed 3 times in PBS (pH 7.4) for 5 min each time, the slides were incubated with secondary antibodies at room temperature for 50 min. The slides were then incubated with DAB solution and counterstained with haematoxylin.

Statistical analysis

The statistical trends of the different groups were analysed with GraphPad Prism 9.5. Data from at least three individual experiments are presented as the means ± standard deviations (means ± SDs). Data were considered statistically significant when $P < 0.05$.

Results

Synthesis of the GelMA/PNS/Alg@IGF-1 hydrogel

The successful synthesis of the GelMA/PNS/Alg@IGF-1 hydrogels was verified through a combination of morphological and structural characterizations. The morphology of the Alg@IGF-1 microspheres was examined via SEM, as shown in Fig. 2A. The microspheres exhibited a spherical shape with a uniform particle size distribution, and the average hydrodynamic diameter was measured to be 48.6 μm (Fig. 2B). The structural modification of the Gel to generate GelMA was confirmed via NMR spectroscopy. Figure 2C shows the NMR spectra of both the Gel and GelMA. Compared with the spectrum of the pure Gel, the spectrum of GelMA exhibited characteristic peaks at δ = 5.4 and 6.4 ppm, which correspond to methacrylate groups. These results clearly demonstrate the successful introduction of methacrylate functional groups and confirm the successful synthesis of GelMA. FTIR spectroscopy was further employed to analyse the chemical composition of the hydrogels, as shown in Fig. 2D. Infrared spectroscopy can detect the characteristic functional groups, molecular structure, and chemical composition of organic compounds. The characteristic absorption peak of the amide bond appeared at 1540 cm^{-1}, which further confirms that GelMA was successfully synthesized. The characteristic absorption peak of PNS appeared at 2927.89 cm^{-1} in GelMA/PNS and GelMA/PNS/Alg@IGF-1, which indicates that PNS was successfully loaded within these two hydrogel samples.

Characteristics of the GelMA/PNS/Alg@IGF-1 hydrogel

The rheological properties of the hydrogels were assessed, and the results are presented in Fig. 2E. G′ and G″ represent the stiffness (storage modulus) and viscoelasticity (loss modulus) of the hydrogel, respectively. G′ was significantly greater than G″ at room temperature for all four hydrogel samples; this finding indicates that the MA material improved the stability of gelatine at room temperature and enabled GelMa to remain in the hydrogel state at body temperature. The compression properties of the hydrogels are shown in Fig. 2F. Following the addition of PNS and Alg@IGF-1, the compressive strength of the hydrogel decreased slightly, but this decrease was not significant.

The swelling behaviour of the hydrogels, shown in Fig. 2G, reflects their fluid absorption and water retention capacities. The swelling ratio increased rapidly during the first 2 h and reached equilibrium at 24 h. The equilibrium swelling ratios of GelMA, GelMA/PNS, GelMA/Alg@IGF-1, and GelMA/PNS/Alg@IGF-1 were 35.51% ± 5.4%, 40.24% ± 1.59%, 70.24% ± 2.70%, and 64.53% ± 2.96%, respectively. The increased swelling ratios of GelMA/Alg@IGF-1 and GelMA/PNS/Alg@IGF-1 were attributed to the hydrophilic properties of alginate in the Alg@IGF-1 microspheres.

The degradation profiles of the hydrogels were evaluated in a lysozyme solution to simulate the in vivo environment, as shown in Fig. 2H. The hydrogels exhibited gradual weight loss due to enzymatic hydrolysis, with residual weights on day 21 of 12.54% ± 3.18%, 13.33% ±

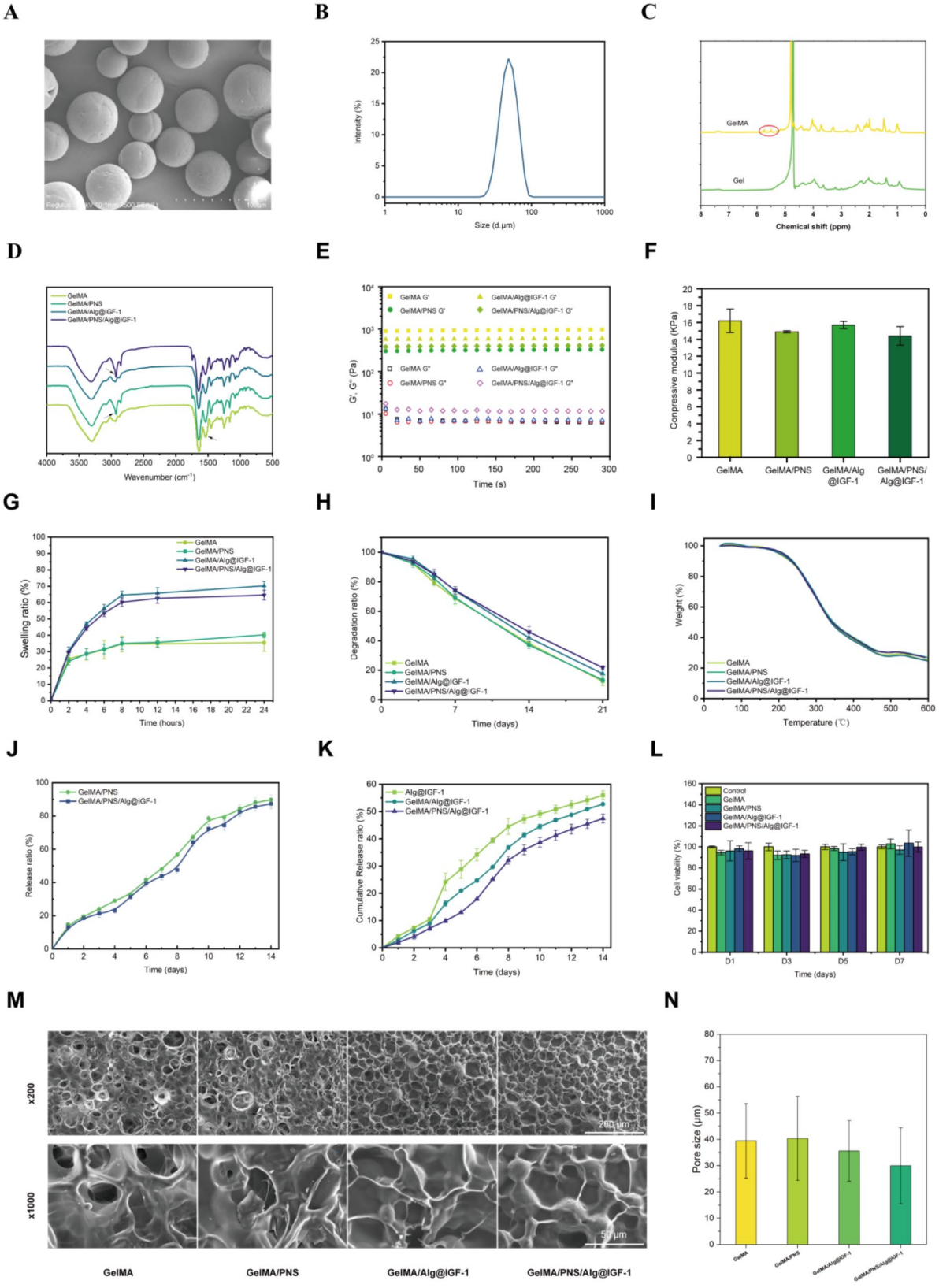

Fig. 2 (See legend on next page.)

(See figure on previous page.)

Fig. 2 Fabrication and physicochemical properties of the hydrogels. SEM images of the microspheres. **B** Particle size distribution of the microspheres. **C** Nuclear magnetic analyses. **D** Fourier transform infrared spectroscopy. **E**, **F**, **G**, **H**, **I** Rheological properties, compressive properties, swelling characteristics, degradation rates, and thermogravimetric analysis of GelMA, GelMA/PNS, GelMA/Alg@IGF-1, and GelMA/PNS/Alg@IGF-1. **J** Release ratios of IGF-1 in Alg@IGF-1, GelMA/Alg@IGF-1 and GelMA/PNS/Alg@IGF-1. **K** Release ratios of PNS in GelMA/PNS and GelMA/PNS/Alg@IGF-1. **L** Biocompatibility test. **M**, **N** SEM images and pore size statistics of the hydrogels

3.35%, 17.61% ± 2.20%, and 21.82% ± 1.24% for GelMA, GelMA/PNS, GelMA/Alg@IGF-1, and GelMA/PNS/Alg@IGF-1, respectively. The GelMA/PNS/Alg@IGF-1 hydrogel exhibited the highest resistance to enzymatic degradation, which indicates its prolonged stability. Thermogravimetric analysis (TGA) (Fig. 2I) revealed that all the GelMA-based materials presented similar thermal degradation profiles, with GelMA/PNS/Alg@IGF-1 displaying slightly greater residual weights, suggesting improved thermal stability due to the incorporation of PNS and IGF-1. These results indicate that the hydrogel formulation offers prolonged functional stability, which would reduce the frequency of dressing replacements.

The release profiles of PNS from the GelMA/PNS and GelMA/PNS/Alg@IGF-1 hydrogels are presented in Fig. 2J. Both hydrogels demonstrated similar sustained-release trends, with release rates of 19.48% ± 0.60% and 18.47% ± 0.69% on day 3 and 88.19% ± 2.78% and 85.59% ± 2.78% on day 14. These findings indicate that the incorporation of Alg@IGF-1 did not affect the release profile of PNS. The sustained release of PNS ensures its presence throughout the wound-healing process and minimizes the need for frequent dressing replacements. The encapsulation efficiency of IGF-1 within Alg@IGF-1 microspheres was 71.81% ± 2.08%. The release rates of IGF-1 from Alg@IGF-1, GelMA/Alg@IGF-1, and GelMA/PNS/Alg@IGF-1 are shown in Fig. 2K. On day 4, the release rates from Alg@IGF-1, GelMA/Alg@IGF-1, and GelMA/PNS/Alg@IGF-1 were 24.18% ± 3.15%, 16.27% ± 0.98%, and 9.88% ± 0.66%, respectively, and by day 14, the release rates were 55.99% ± 1.60%, 52.72% ± 0.21%, and 47.42% ± 1.60%, respectively. The slower release rates of the GelMA-based hydrogels suggest a more controlled and sustained release of IGF-1 and ensure its availability during the middle and late stages of wound healing.

The cytocompatibility of the hydrogels was evaluated via a CCK-8 assay using fibroblasts cultured for 1, 3, and 5 days. As shown in Fig. 2L, no significant differences in cell viability were observed among the GelMA, GelMA/PNS, GelMA/Alg@IGF-1, GelMA/PNS/Alg@IGF-1, and control groups, which indicates excellent biocompatibility of the hydrogels for direct application to wound surfaces. SEM analysis revealed that all the hydrogel samples exhibited a spongy 3D porous structure, with Alg@IGF-1 microspheres embedded within the GelMA/Alg@IGF-1 and GelMA/PNS/Alg@IGF-1 hydrogels (Fig. 2M). The average pore sizes for GelMA, GelMA/PNS, GelMA/Alg@IGF-1, and GelMA/PNS/Alg@IGF-1 were 39.47 ± 14.14 μm, 40.39 ± 16.00 μm, 35.63 ± 11.54 μm, and 29.97 ± 14.46 μm, respectively, and no significant differences were observed among the different hydrogels (Fig. 2N).

Angiogenic effect of the GelMA/PNS/Alg@IGF-1 hydrogel under High-Glucose conditions

To explore abnormalities in the wound healing process of diabetic wounds, we cultured HUVECs in high-glucose medium to mimic diabetic conditions in vitro. The initial assessment of HUVEC viability in a high-glucose (HG) environment revealed that prolonged exposure significantly damaged the cells and induced apoptosis. However, all the treatment groups demonstrated varying degrees of restored cell viability, and the GelMA/PNS/Alg@IGF-1 hydrogel group showed the most pronounced antiapoptotic effect (Fig. 3A, B). The migration and tube formation of endothelial cells are critical steps needed to achieve therapeutic effects. Under the influence of a high-glucose environment, HUVEC migration and tube formation abilities are significantly impaired. However, treatment with the GelMA/PNS/Alg@IGF-1 hydrogel markedly restored HUVEC migration, which was superior to that of cells treated with other hydrogels and resulted in the formation of a more distinct vascular network (Fig. 3C-F).

To further investigate the potential mechanisms by which the GelMA/PNS/Alg@IGF-1 hydrogel promotes vascularization, we performed transcriptome sequencing of HUVECs. Compared with the high-glucose-treated cells, the GelMA/PNS/Alg@IGF-1 hydrogel-treated cells presented significant changes in gene transcription, with a total of 2,642 differentially expressed genes (DEGs) identified. Among these genes, 554 genes were upregulated, and 2,088 genes were downregulated (Fig. 3G, H). To gain deeper insight into the functional significance of these DEGs, we performed KEGG pathway enrichment analysis. The enriched pathways were predominantly related to the TNF signalling pathway, NF-kappa B signalling pathway, apoptosis pathway, P53 signalling pathway, and NOD-like receptor signalling pathway (Fig. 3I). We also classified the DEGs through GO pathway analysis and focused on three main domains: biological process (BP), molecular function (MF), and cellular component (CC) (Fig. 3J). In the BP category, the DEGs were enriched primarily in pathways related to the response to stress and the response to cytokines, which highlights the hydrogel's ability to modulate endothelial

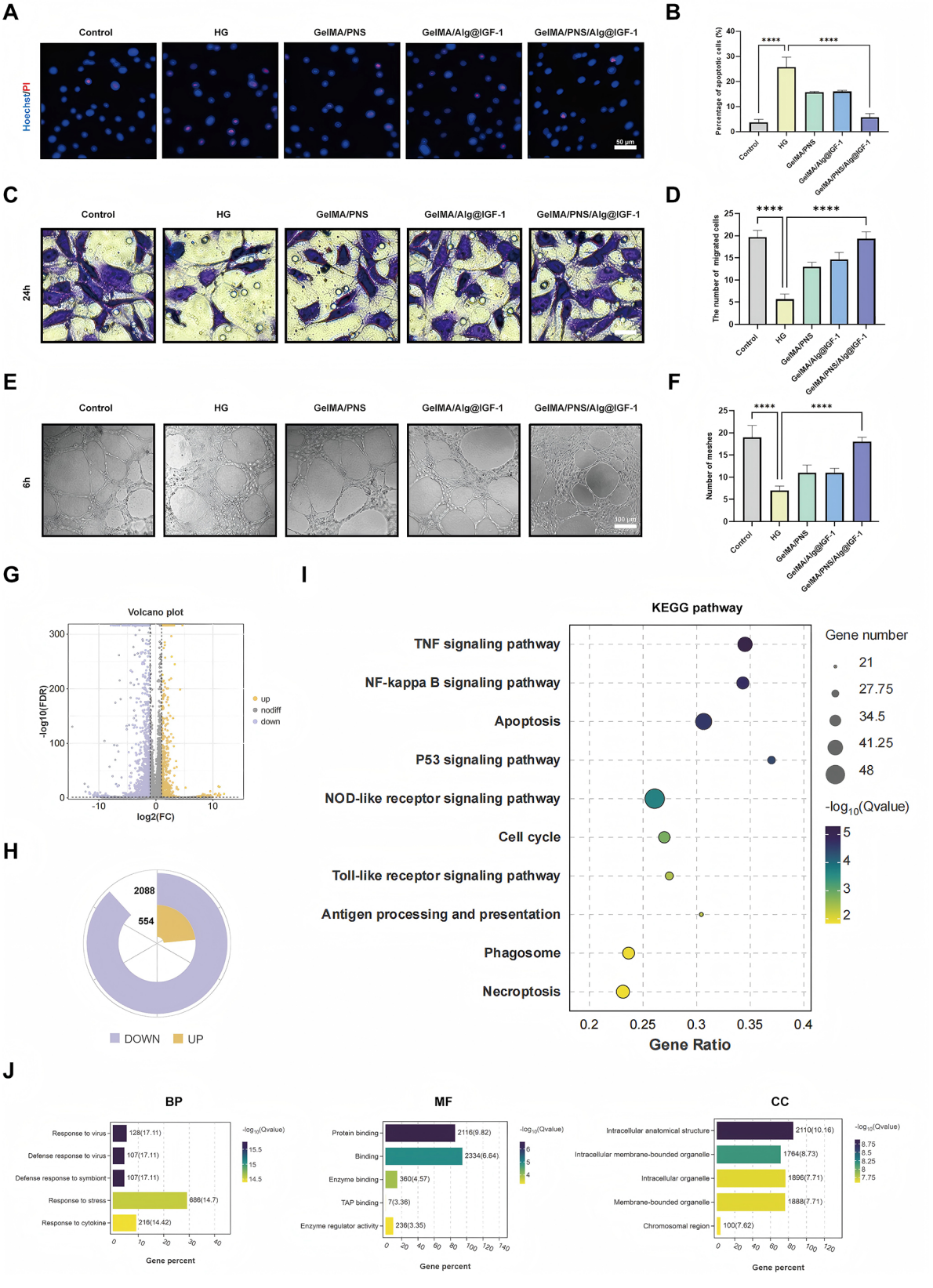

Fig. 3 (See legend on next page.)

(See figure on previous page.)

Fig. 3 Effect of the GelMA/PNS/Alg@IGF-1 hydrogel on angiogenesis under high-glucose conditions. **A, B** Representative fluorescence images and statistical analysis of cell apoptosis. **C, D** Representative images and statistical analysis of cell migration. **E, F** Representative images and statistical analysis of the results of the tube formation assay. **G** Volcano map of the differentially expressed genes between the high glucose (HG)-treated group and the GelMA/PNS/Alg@IGF-1 hydrogel-treated group. **H** Statistical plot of the differentially expressed genes. **I** KEGG pathway enrichment factor map of the differentially expressed genes. **J** GO pathway enrichment factor map of the differentially expressed genes. (**** indicates $p < 0.001$)

cell adaptive responses under pathological conditions. For the MF domain, the most enriched terms were binding and protein binding, which suggests that the hydrogel might regulate interactions between key proteins and signalling molecules and potentially contribute to enhanced cell communication and function. In the CC domain, the DEGs were enriched mainly in intracellular anatomical structures and intracellular membrane-bound organelles, indicating the impact of the hydrogel on intracellular organization and membrane dynamics.

Target analysis of the PNS and IGF-1 in relation to diabetic wounds

On the basis of the above findings, we discovered that the combined delivery of IGF-1 and PNS can exert a more potent proangiogenic effect. Considering the increasing availability of various target databases, bioinformatics approaches were utilized to further explore the connection between these agents and diabetic wound healing. First, we retrieved potential targets for PNS from the HERB, TCMSP, and STP databases. After merging the results, we identified a total of 96 target genes associated with PNS (Fig. 4A and Supplementary Information 1). These 96 genes were enriched primarily in pathways such as the PI3K-Akt signalling pathway and cellular senescence (Fig. 4B), which suggests that PNS may play a role in regulating cell survival, proliferation, and ageing, which are critical for wound repair. In parallel, we utilized several disease-related databases, including OMIM, GeneCards, DRUGBANK, DisGeNet, and TTD, to identify 3,207 key target genes associated with diabetic wounds or diabetic ulcers (Fig. 4C and Supplementary Information 1). By performing an intersection analysis between these 3,207 targets and the 96 PNS-related targets using a Venn diagram, we identified 66 overlapping genes for subsequent bioinformatics analysis (Fig. 4D). These shared targets suggest that the therapeutic effects of PNS on diabetic wounds occur primarily through pathways such as the PI3K−Akt signalling pathway and cellular senescence (Fig. 4E).

Furthermore, we employed the GeneMANIA database to visualize the interaction network of IGF-1 (Fig. 4F). Enrichment analysis of the downstream targets of IGF-1 revealed that IGF-1 is predominantly involved in regulating pathways such as the longevity regulating pathway, the AMPK signalling pathway, and the FoxO signalling pathway (Fig. 4G). Notably, the involvement of pathways such as cellular senescence and longevity regulation suggest that IGF-1 and PNS may mitigate the adverse effects of cellular ageing on wound repair, addressing a critical challenge in the context of diabetes.

Anti-Senescence activity of the GelMA/PNS/Alg@IGF-1 hydrogel

Guided by bioinformatics findings, we investigated the anti-senescence effects of the GelMA/PNS/Alg@IGF-1 hydrogel on endothelial cells under high-glucose conditions. Senescence in HUVECs was assessed by staining for SA-β-gal, a widely recognized marker of cellular senescence. The HG group displayed intense SA-β-gal staining (Fig. 5A), which indicates a robust induction of senescence. In contrast, cells treated with various hydrogels presented reduced SA-β-gal staining, with the GelMA/PNS/Alg@IGF-1 hydrogel demonstrating the most pronounced suppression of senescence (Fig. 5B). At the molecular level, this hydrogel significantly downregulated the mRNA expression of the key senescence markers p21 and p53 and also suppressed the secretion of factors associated with senescence-associated secretory phenotypes (SASPs), such as IL-1β and IL-6 (Fig. 5G, H). These results indicate that the GelMA/PNS/Alg@IGF-1 hydrogel alleviates both cellular senescence and the associated inflammatory microenvironment. Mitochondria, which are central to cellular homeostasis, are directly involved in the senescence process [28, 29]. High-glucose conditions disrupt mitochondrial function, leading to increased ROS production and a loss of mitochondrial membrane potential, both of which are hallmarks of cellular ageing [28, 29]. Our results also reveal that the GelMA/PNS/Alg@IGF-1 hydrogel significantly suppressed HG-induced ROS overproduction while restoring the mitochondrial membrane potential (Fig. 5C-F).

Further GSEA revealed that treatment with the GelMA/PNS/Alg@IGF-1 hydrogel under high-glucose conditions significantly activated oxidative phosphorylation pathways but inhibited the NF-κB signalling pathway (Fig. 5I, J). The western blot results further confirmed that under high-glucose conditions, total IκBα protein levels were decreased, phosphorylated IκBα (p-IκBα) levels were increased, total p65 protein levels remained unchanged, and phosphorylated p65 (p-p65) levels were increased. However, intervention with the GelMA/PNS/Alg@IGF-1 hydrogel reversed this effect by suppressing the phosphorylation of both IκB-α and p65, thereby preventing excessive activation of the NF-κB signalling pathway (Fig. 5K). These findings demonstrate that the

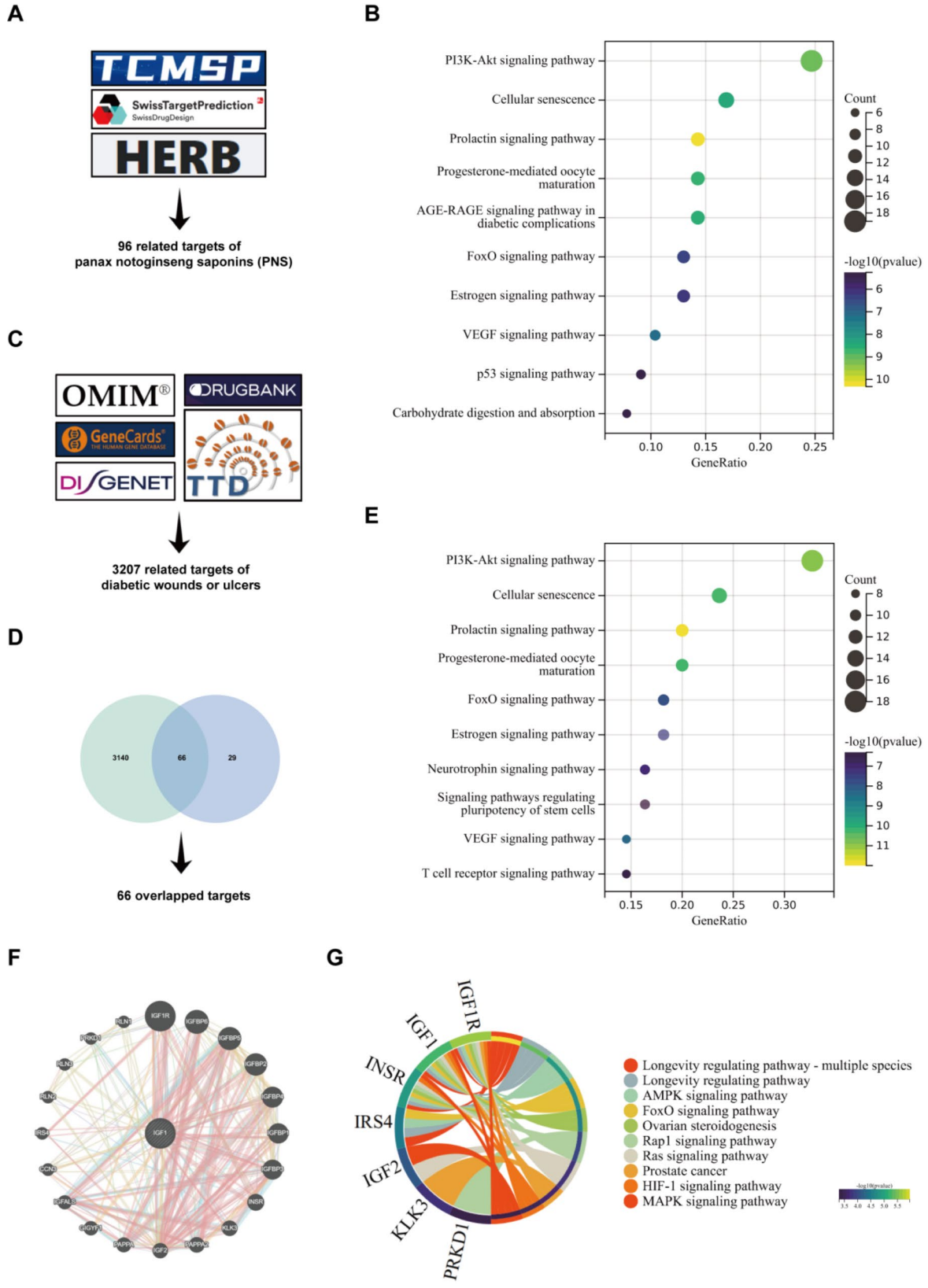

Fig. 4 Analysis of the PNS and IGF-1 targets via network pharmacology. **A** Schematic diagram of target screening for PNS. **B** KEGG pathway enrichment analysis of PNS targets. **C** Schematic diagram of target screening for diabetic wounds or ulcers. **D** Summary of target genes from multiple databases. **E** KEGG pathway enrichment analysis of overlapping targets. **F** Schematic diagram of key interacting targets of IGF-1. **G** KEGG pathway enrichment analysis of key interacting targets of IGF-1

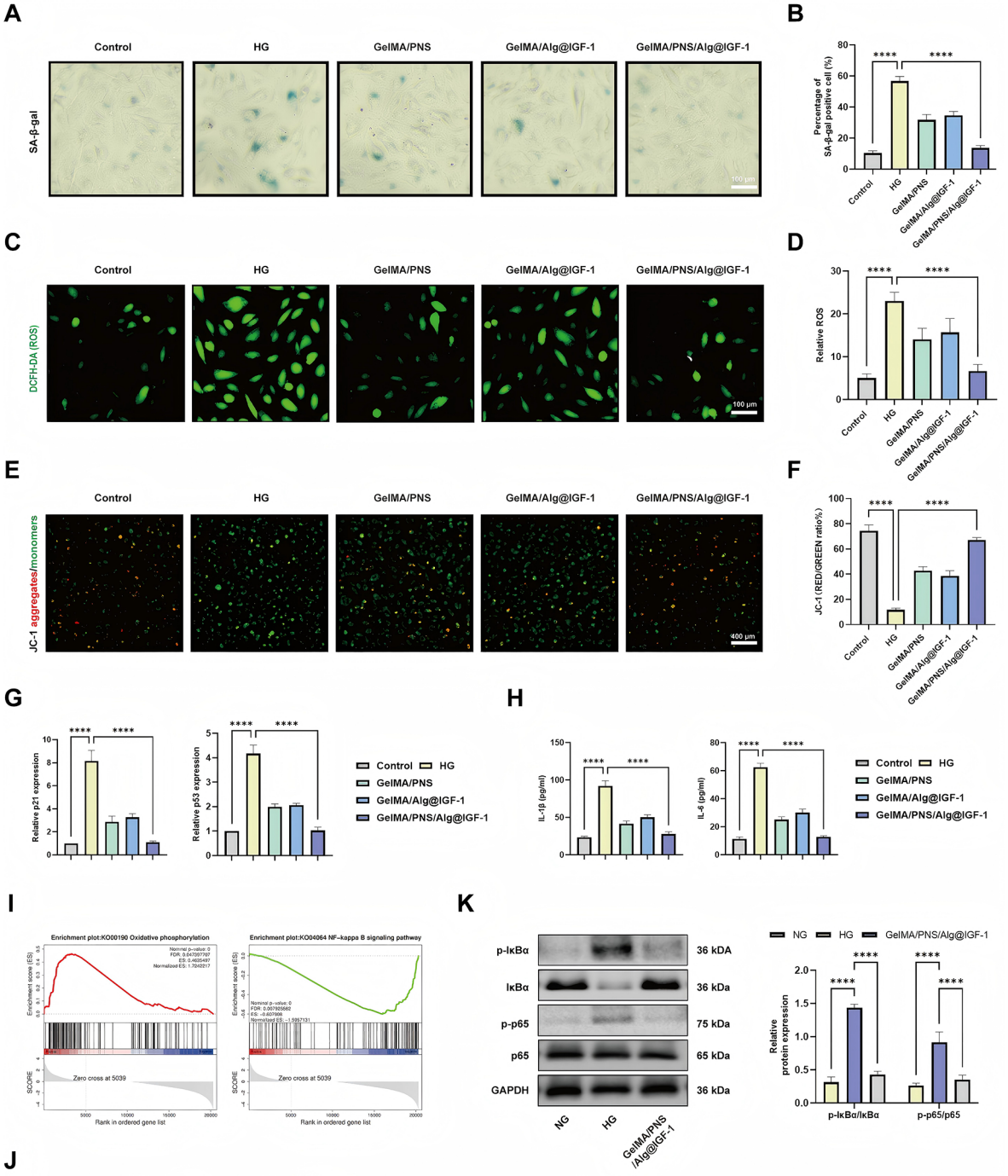

Fig. 5 (See legend on next page.)

(See figure on previous page.)

Fig. 5 Anti-senescence effects of the GelMA/PNS/Alg@IGF-1 hydrogel in a high-glucose environment. **A, B** Representative images and statistical analysis of SA-β-gal staining. **C, D** Representative images and statistical analysis of ROS fluorescence staining. **E, F** Representative images and statistical analysis of mitochondrial membrane potential fluorescence staining. **G** RT–qPCR analysis of senescence markers (p21 and p53). **H** ELISA analysis of factors associated with SASPs (IL-1β and IL-6). **I** GSEA comparing the high glucose (HG)-treated group and the GelMA/PNS/Alg@IGF-1 hydrogel-treated group. **J** Heatmap of gene expression related to the NF-κB signalling pathway in the HG-treated group and the GelMA/PNS/Alg@IGF-1 hydrogel-treated group. **K** Western blot bands and quantitative analysis of the expression of proteins in the NF-κB signalling pathway. (** indicates $P < 0.01$, **** indicates $P < 0.001$)

GelMA/PNS/Alg@IGF-1 hydrogel mitigates oxidative stress, restores mitochondrial function, and suppresses senescence signalling through the NF-κB pathway.

In vivo wound healing effects of the GelMA/PNS/Alg@IGF-1 hydrogel

The wound healing efficacy of the GelMA/PNS/Alg@IGF-1 hydrogel was evaluated in a diabetic skin wound model. Figure 6A outlines the in vivo treatment strategy. Representative images of the healing process are shown in Fig. 6B. Compared with those in the control group, the wounds treated with the GelMA/PNS, GelMA/Alg@IGF-1, and GelMA/PNS/Alg@IGF-1 hydrogels exhibited more rapid healing progression (Fig. 6C). Notably, the GelMA/PNS/Alg@IGF-1 group demonstrated the most pronounced increase in wound healing (Fig. 6D). While the GelMA/PNS and GelMA/Alg@IGF-1 hydrogel groups demonstrated significantly faster healing than the control, their healing rates were still less than the healing rate of the GelMA/PNS/Alg@IGF-1 hydrogel group. These findings suggest that the combined application of PNS and IGF-1 within the hydrogel synergistically promote diabetic wound healing more effectively than either agent alone.

To further evaluate the wound healing process, histological analysis was conducted on days 7 and 14. Figure 6E shows HE-stained skin tissue. Compared with the other groups, the GelMA/PNS/Alg@IGF-1 hydrogel group exhibited a higher rate of granulation tissue formation on day 7 (Fig. 6F). By day 14, all the groups presented a newly formed epidermis; however, the GelMA/PNS/Alg@IGF-1 hydrogel group presented a thicker, more natural, and mature epidermal layer than the other groups (Fig. 6G). Collagen deposition, a critical factor in wound remodelling, was assessed via Masson's trichrome staining (Fig. 6H). Compared with the control group, all the treatment groups presented increased collagen content. However, compared with the other groups, the GelMA/PNS/Alg@IGF-1 hydrogel group presented significantly greater collagen deposition on both day 7 and day 14 (Fig. 6I). These findings indicate that this hydrogel formulation not only accelerates granulation tissue formation and re-epithelialization but also enhances collagen synthesis and remodelling, which are essential for robust wound healing.

To evaluate the angiogenic potential of the hydrogel in vivo, we assessed the expression levels of CD31, a key marker associated with angiogenesis (Fig. 6J). CD31 staining revealed significantly greater neovascularization in wounds treated with the GelMA/PNS/Alg@IGF-1 hydrogel than in those in the control group (Fig. 6K). This significant increase demonstrates that the GelMA/PNS/Alg@IGF-1 hydrogel effectively promotes angiogenesis, which addresses the angiogenic deficiencies in diabetic wounds. The synergistic combination of PNS and IGF-1 establishes a favourable microenvironment for angiogenesis and facilitates efficient and complete tissue repair.

Anti-Senescence effects of the GelMA/PNS/Alg@IGF-1 hydrogel on angiogenesis

Measurements of ROS levels in in vivo experiments revealed that all hydrogel formulations reduced oxidative stress and that the GelMA/PNS/Alg@IGF-1 hydrogel exhibited the most pronounced antioxidant effect (Fig. 7A, B). This reduction in oxidative stress plays a pivotal role in improving vascular function. CD31/α-SMA double immunofluorescence staining further confirmed the proangiogenic effects of this hydrogel. Compared with wounds treated with other hydrogels, wounds treated with the GelMA/PNS/Alg@IGF-1 hydrogel presented a significantly greater number of mature blood vessels throughout the healing process, which highlights the ability of this hydrogel to promote sustained angiogenesis (Fig. 7C, D and Supplementary Fig. 1).

To further investigate its anti-senescence effects, IHC was used to assess the expression of the senescence marker p16 and factors associated with SASPs, including IL-6 and TNF-α. Although the expression of these markers was reduced in all treatment groups, the GelMA/PNS/Alg@IGF-1 hydrogel exhibited the most significant suppressive effects (Fig. 7E, F). Additionally, during the wound healing process, the expression levels of TGF-β1 and TGF-β3 were notably greater in wounds treated with the GelMA/PNS/Alg@IGF-1 hydrogel than in the other groups (Fig. 7G, H). The elevated levels of these growth factors suggest that this hydrogel further enhances angiogenesis by establishing a pro-healing microenvironment that supports both structural and functional recovery of the vasculature.

Discussion

This study demonstrated that the multifunctional GelMA/PNS/Alg@IGF-1 hydrogel effectively addresses key pathological features of diabetic wounds, including

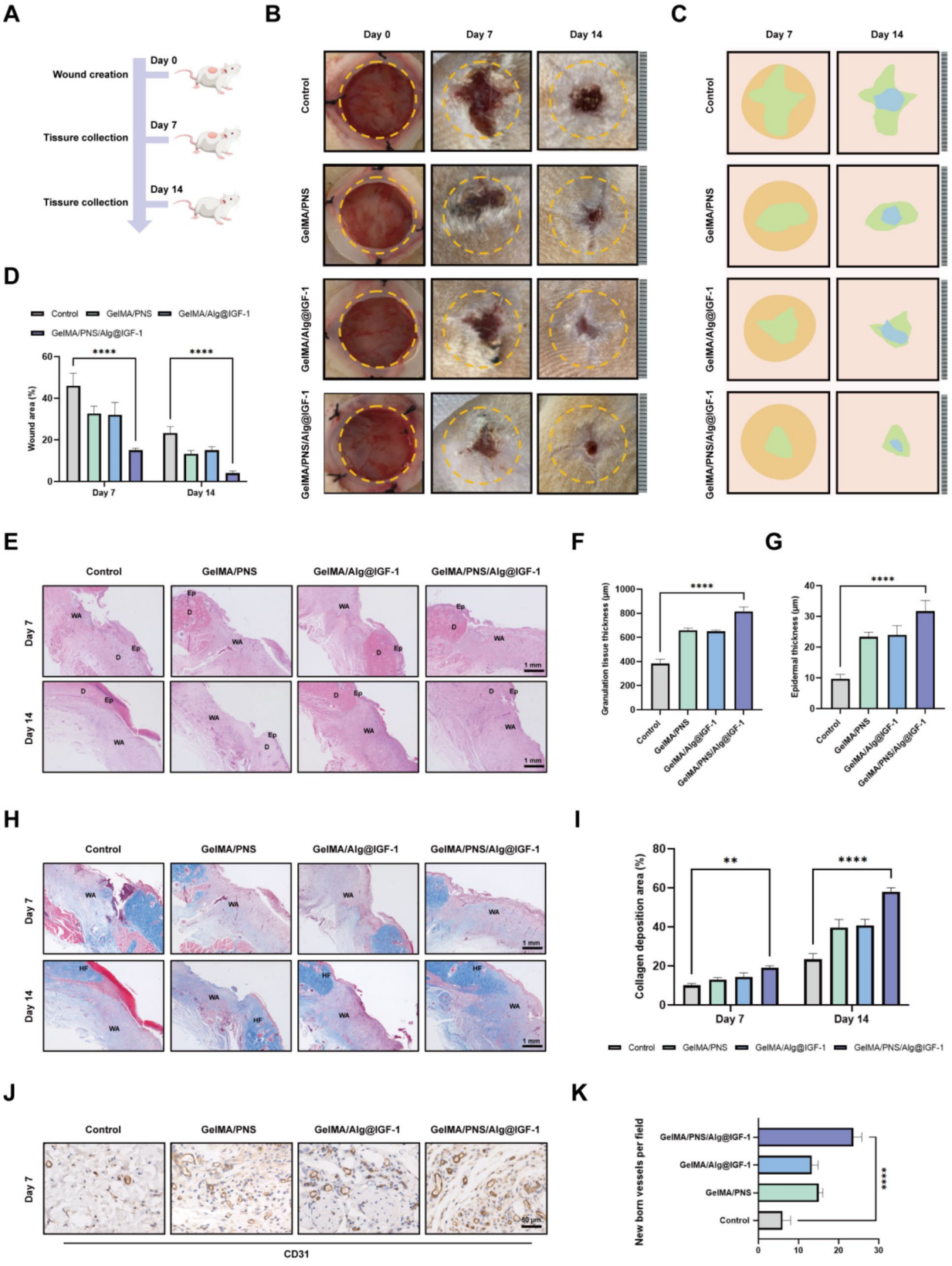

Fig. 6 (See legend on next page.)

(See figure on previous page.)

Fig. 6 In vivo evaluation of the effects of different hydrogels on diabetic wound healing. **A** Treatment schedule for diabetic wounds treated with different hydrogels. **B, C** Representative images and wound healing trajectories of diabetic wounds at various time points. **D** Quantitative analysis of wound healing rates after treatment. **E** HE staining of wound sections from all groups on days 7 and 14. (WA: Wound Area, Ep: Epidermis, D: Dermis). **F** Statistical analysis of granulation tissue thickness on day 7. **G** Quantitative analysis of epidermal thickness on day 14. **H** Masson staining images of wounds from all groups on days 7 and 14. (WA: Wound Area, HF: Hair follicle). **I** Quantification of collagen deposition on days 7 and 14. **J, K** Images of immunohistochemical staining and statistical analysis showing CD31-labelled neovasculature in wound tissues on day 7. (** indicates $P < 0.01$, **** indicates $P < 0.001$)

oxidative stress, cellular senescence, and impaired angiogenesis. By combining PNS and IGF-1 in a hydrogel platform with controlled release properties, this formulation provides synergistic therapeutic effects and establishes a favourable microenvironment for tissue repair and regeneration.

The successful synthesis and characterization of the GelMA/PNS/Alg@IGF-1 hydrogel confirmed its structural stability, biocompatibility, and suitability for wound healing applications. The rheological and degradation properties demonstrated its ability to remain stable during wound healing, while the controlled release of PNS and IGF-1 over 14 days minimized the need for frequent dressing replacements. The optimal swelling ratios and pore sizes support a moist wound environment and facilitate cell migration, both of which are critical for wound healing and tissue regeneration [30, 31].

High glucose levels impair vascular function in diabetic wounds, which contributes to delayed healing and chronic inflammation [32, 33]. The GelMA/PNS/Alg@IGF-1 hydrogel significantly improved endothelial cell viability, migration, and tube formation under high-glucose conditions, which indicates its ability to restore vascular function. Transcriptome analysis revealed that this hydrogel modulates vascular repair through pathways such as the NF-κB, PI3K-Akt, and TNF signalling pathways. These pathways are crucial for promoting endothelial cell survival, neovascularization, and wound repair, as they reduce inflammation and enhance adaptive cellular responses to stress [34, 35]. The integration of bioinformatics and experimental data provides valuable insights into the molecular mechanisms that drive the therapeutic effects of PNS and IGF-1.

Cellular senescence induced by high-glucose conditions is a major factor that inhibits wound healing in diabetic patients [36–38]. The network pharmacology results revealed that PNS and IGF-1 have significant anti-senescence potential. The GelMA/PNS/Alg@IGF-1 hydrogel effectively suppressed the expression of HG-induced markers of senescence (SA-β-gal, p21, p53) and SASPs (IL-1β, IL-6), alleviating the proinflammatory microenvironment associated with senescence. The ability of the hydrogel to reduce ROS production and restore the mitochondrial membrane potential underscores its capacity to disrupt the cycle of oxidative stress and mitochondrial dysfunction that perpetuate cellular ageing [28, 29]. Western blot results further confirmed the dissociation of the NF-κB/IκB-α complex and the activation of the NF-κB signalling pathway under high-glucose conditions [39, 40]. The NF-κB pathway plays a crucial role in inflammation and senescence-associated dysfunctions [41]. By inhibiting NF-κB signalling, the hydrogel further mitigated the feedback loop between oxidative stress and senescence-associated inflammation, promoting vascular repair [39, 42, 43].

As previously mentioned, wound healing is a complex and dynamic process involving multiple stages, including inflammation, granulation tissue formation, re-epithelialization, and collagen remodelling [44]. The rapid development of advanced biomaterials has led to faster and more effective wound healing [45, 46]. Insufficient angiogenesis caused by pathological factors is a common characteristic of diabetic wounds, which highlights the importance of angiogenesis in tissue repair [47, 48]. The diabetic wound model demonstrated that the GelMA/PNS/Alg@IGF-1 hydrogel significantly accelerated wound healing, as evidenced by enhanced granulation tissue formation, collagen deposition, and re-epithelialization. The upregulation of angiogenic markers such as CD31 confirmed the efficacy of this hydrogel in promoting neovascularization, a critical factor for oxygen and nutrient delivery to healing tissues [49, 50]. More importantly, hydrogels not only alleviate senescence in the wound environment but also reduce the inflammatory microenvironment associated with SASP-related factor secretion, which is essential for promoting angiogenesis and facilitating wound repair [51].

Recent studies highlight the promising potential of advanced dual-delivery biomaterials in wound healing. For example, platelet-rich fibrin and simvastatin-loaded 3D-printed bilayer scaffolds promote angiogenesis and cellular proliferation for skin regeneration [52]. Similarly, vanillin- and IGF-1-loaded dual-layer wound dressings enhance cell migration, angiogenesis, and collagen deposition to accelerate healing [53]. The dual delivery of PNS and IGF-1 produced a synergistic effect and established a favourable microenvironment for vascular repair and tissue remodelling. Increased levels of TGF-β1 and TGF-β3 further support the ability of our hydrogel to regulate inflammation resolution and promote extracellular matrix remodelling, which are both essential for robust and sustained healing [54, 55]. These findings highlight the effectiveness of multitargeted therapies combined with advanced biomaterials for optimal wound

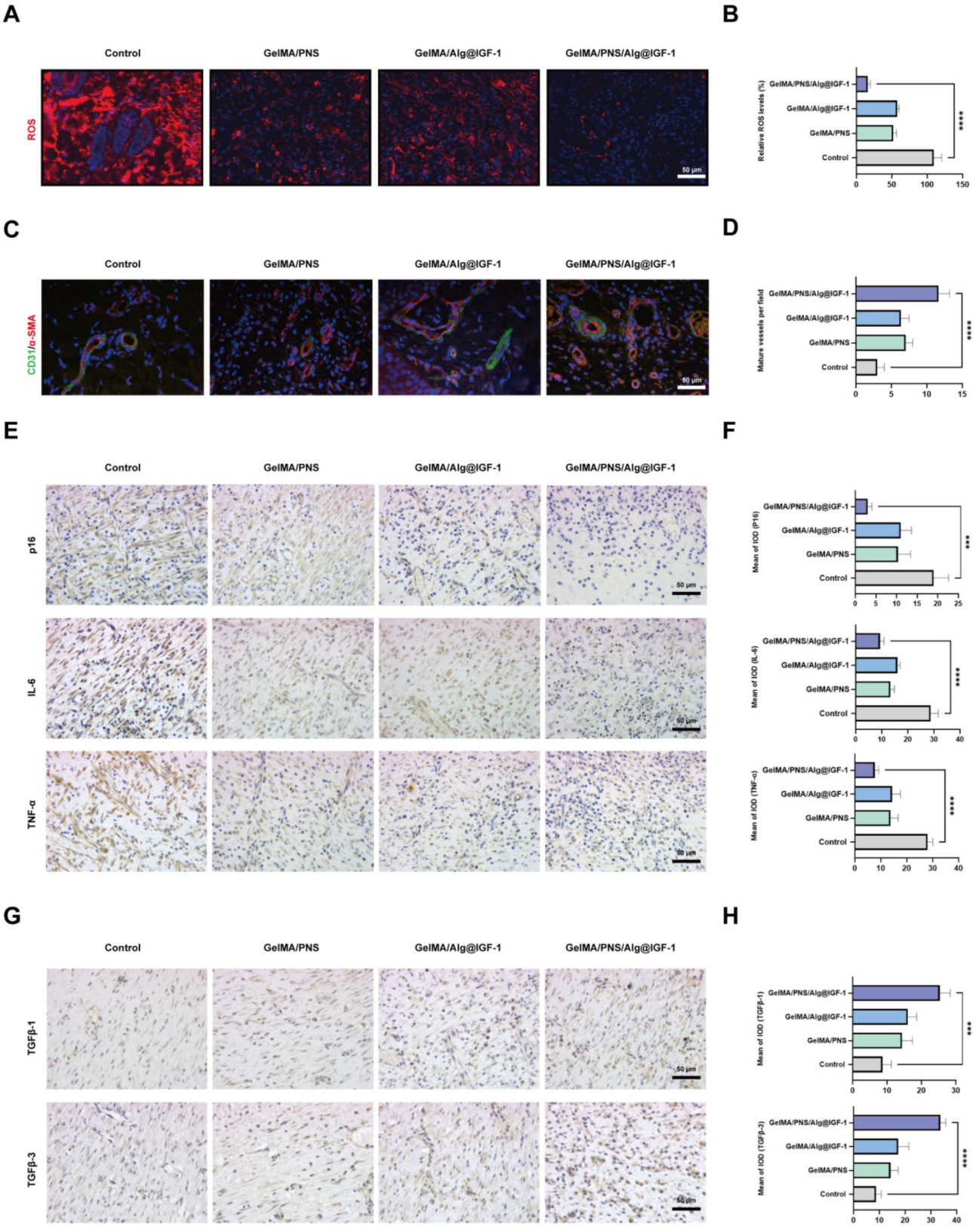

Fig. 7 (See legend on next page.)

(See figure on previous page.)

Fig. 7 Anti-senescence and proangiogenic effects of the GelMA/PNS/Alg@IGF-1 hydrogel. **A, B** Representative images and quantitative measurements of ROS levels in the wounds of different treatment groups. **C, D** Images of CD31/α-SMA double immunofluorescence staining and quantitative analysis of mature blood vessels. **E, F** Images of immunohistochemical staining and quantitative analysis of the senescence marker p16 and factors associated with SASPs (IL-6 and TNF-α) in wound tissues. **G, H** Images of immunohistochemical staining and quantitative analysis of TGF-β1 and TGF-β3 expression levels in wound tissues. (*** indicates $P < 0.005$, **** indicates $P < 0.001$)

healing. Expanding the multifunctionality of biomaterials and diversifying their applications to address a broader disease spectrum represent a critical focus for future research and development [56, 57].

Due to its anti-senescence and proangiogenic properties, the GelMA/PNS/Alg@IGF-1 hydrogel offers a promising therapeutic strategy for the management of diabetic wounds by addressing the challenges of delayed healing and chronic inflammation. While the encouraging in vitro and in vivo results highlight its potential, further studies are necessary to assess its long-term safety, scalability, and clinical efficacy. Evaluations in larger animal models and eventual clinical trials will be crucial for translating this innovative platform into practical applications for chronic wound management. By effectively targeting oxidative stress, cellular senescence, and impaired angiogenesis, the GelMA/PNS/Alg@IGF-1 hydrogel has strong potential as a multifunctional solution for advanced wound care.

Supplementary Information

The online version contains supplementary material available at https://doi.org/10.1186/s12951-025-03274-5.

Supplementary Material 1

Supplementary Material 2

Supplementary Material 3

Supplementary Material 4

Acknowledgements
The present work is the result of multiple joint efforts. We wish to express our sincere appreciation to all those who offered invaluable support during this study. Flow chart mapping was assisted by Biorender.

Author contributions
Hao Yang: Data curation, Formal analysis, Investigation, Methodology, Writing – original draft. Yongfei Chen: Investigation, Data curation, Validation. Yanchao Rong: Methodology, Data curation, Validation. Yuxi Zhou: Investigation, Formal analysis, Resources. Shuting Li: Methodology, Formal analysis, Validation. Xiaohui Li: Resources. Honglin Wu: Resources. Dongming Lv: Resources. Xiaoling Cao: Formal analysis. Peng Wang: Validation. Jiayuan Zhu: Conceptualization, Funding acquisition, Supervision, Resources. Bing Tang: Conceptualization, Funding acquisition, Supervision, Resources. Zhicheng Hu: Conceptualization, Methodology, Funding acquisition, Supervision, Writing – review & editing. All authors read and approved the final manuscript.

Funding
This work was supported in part by the National Natural Science Foundation of China (82172213, 82072181, and 82072180) and the Guangdong Provincial Natural Science Foundation of China (2024A1515010485).

Data availability
No datasets were generated or analysed during the current study.

Declarations

Ethics approval and consent to participate
This study was approved by the ICE for Clinical Research and Animal Trials of the First Affiliated Hospital of Sun Yat-sen University. Approval No: (2021)860.

Competing interests
The authors declare no competing interests.

Author details
[1]Department of Burn and Wound Repair, First Affiliated Hospital of Sun Yat-sen University, Guangzhou 510080, China
[2]Department of Plastic Surgery, First Affiliated Hospital of Sun Yat-sen University, Guangzhou 510080, China

Received: 25 January 2025 / Accepted: 24 February 2025
Published online: 06 March 2025

References

1. Zhao R, Liang H, Clarke E, Jackson C, Xue M. Inflammation in chronic wounds. Int J Mol Sci. 2016;17.
2. Sena CM, Pereira AM, Seiça R. Endothelial dysfunction - a major mediator of diabetic vascular disease. Biochim Biophys Acta. 2013;1832:2216–31.
3. Wilkinson HN, Hardman MJ. Senescence in wound repair: emerging strategies to target chronic healing wounds. Front Cell Dev Biol. 2020;8:773.
4. Pitocco D, Zaccardi F, Di Stasio E, Romitelli F, Santini SA, Zuppi C, Ghirlanda G. Oxidative stress, nitric oxide, and diabetes. Rev Diabet Stud. 2010;7:15–25.
5. Guo S, Dipietro LA. Factors affecting wound healing. J Dent Res. 2010;89:219–29.
6. Annabi N, Tamayol A, Uquillas JA, Akbari M, Bertassoni LE, Cha C, Camci-Unal G, Dokmeci MR, Peppas NA, Khademhosseini A. 25th anniversary Article: rational design and applications of hydrogels in regenerative medicine. Adv Mater. 2014;26:85–123.
7. Djagny VB, Wang Z, Xu S. Gelatin: a valuable protein for food and pharmaceutical industries: review. Crit Rev Food Sci Nutr. 2001;41:481–92.
8. Nichol JW, Koshy ST, Bae H, Hwang CM, Yamanlar S, Khademhosseini A. Cell-laden microengineered gelatin methacrylate hydrogels. Biomaterials. 2010;31:5536–44.
9. Chen X, Du W, Cai Z, Ji S, Dwivedi M, Chen J, Zhao G, Chu J. Uniaxial stretching of Cell-Laden microfibers for promoting C2C12 myoblasts alignment and myofibers formation. ACS Appl Mater Interfaces. 2020;12:2162–70.
10. Cho JY, Yoo ES, Baik KU, Park MH, Han BH. In vitro inhibitory effect of Protopanaxadiol ginsenosides on tumor necrosis factor (TNF)-alpha production and its modulation by known TNF-alpha antagonists. Planta Med. 2001;67:213–8.
11. Zhang E, Gao B, Yang L, Wu X, Wang Z. Notoginsenoside Ft1 promotes fibroblast proliferation via PI3K/Akt/mTOR signaling pathway and benefits wound healing in genetically diabetic mice. J Pharmacol Exp Ther. 2016;356:324–32.
12. Atanasova M, Whitty A. Understanding cytokine and growth factor receptor activation mechanisms. Crit Rev Biochem Mol Biol. 2012;47:502–30.
13. Zubair M, Ahmad J. Role of growth factors and cytokines in diabetic foot ulcer healing: A detailed review. Rev Endocr Metab Disord. 2019;20:207–17.
14. Al-Sudani BT, Salehi S, Kamil MM, Al-Musawi MH, Valizadeh H, Mirhaj M, Sharifianjazi M, Shahriari-Khalaji M, Sattar M, Sharifianjazi F, et al. Highly porous 3D printed scaffold incorporated with graphene Oxide-Merwinite and coated with IGF1 loaded nanofibers for calvarial defect repair. J Polym Environ. 2024;32:5330–43.
15. He Y, Li H, Zheng X, Yuan M, Yang R, Yuan M, Yang C. Preparation, in vivo and in vitro release of polyethylene glycol monomethyl Ether-Polymandelic acid microspheres loaded Panax Notoginseng saponins. Molecules. 2019;24.
16. Mitchell AC, Briquez PS, Hubbell JA, Cochran JR. Engineering growth factors for regenerative medicine applications. Acta Biomater. 2016;30:1–12.

17. Zaman R, Islam RA, Ibnat N, Othman I, Zaini A, Lee CY, Chowdhury EH. Current strategies in extending half-lives of therapeutic proteins. J Control Release. 2019;301:176–89.
18. Al-Musawi MH, Turki S, Al-Naymi HAS, Sameer Al-salman S, Boroujeni VV, Alizadeh M, Sattar M, Sharifianjazi F, Bazli L, Pajooh AMD, et al. Localized delivery of healing stimulator medicines for enhanced wound treatment. J Drug Deliv Sci Technol. 2024;101:106212.
19. Al-Naymi H, Al-Musawi MH, Mirhaj M, Valizadeh H, Momeni A, Danesh PA, Shahriari-Khalaji M, Sharifianjazi F, Tavamaishvili K, Kazemi N, et al. Exploring nanobioceramics in wound healing as effective and economical alternatives. Heliyon. 2024;10:e38497.
20. Saghazadeh S, Rinoldi C, Schot M, Kashaf SS, Sharifi F, Jalilian E, Nuutila K, Giatsidis G, Mostafalu P, Derakhshandeh H, et al. Drug delivery systems and materials for wound healing applications. Adv Drug Deliv Rev. 2018;127:138–66.
21. Boateng JS, Matthews KH, Stevens HN, Eccleston GM. Wound healing dressings and drug delivery systems: a review. J Pharm Sci. 2008;97:2892–923.
22. Kim HS, Sun X, Lee JH, Kim HW, Fu X, Leong KW. Advanced drug delivery systems and artificial skin grafts for skin wound healing. Adv Drug Deliv Rev. 2019;146:209–39.
23. Gupta V, Khan Y, Berkland CJ, Laurencin CT, Detamore MS. Microsphere-Based scaffolds in regenerative engineering. Annu Rev Biomed Eng. 2017;19:135–61.
24. Farasatkia A, Kharaziha M, Ashrafizadeh F, Salehi S. Transparent silk/gelatin methacrylate (GelMA) fibrillar film for corneal regeneration. Mater Sci Eng C Mater Biol Appl. 2021;120:111744.
25. Dhamecha D, Movsas R, Sano U, Menon JU. Applications of alginate microspheres in therapeutics delivery and cell culture: past, present and future. Int J Pharm. 2019;569:118627.
26. Jahani M, Asefnejad A, Al-Musawi MH, Mohammed AA, Al-Sudani BT, Hameed AM, Kadhim NA, Shahriari-Khalaji M, Valizadeh H, Sharifianjazi F, et al. Antibacterial and wound healing stimulant nanofibrous dressing consisting of soluplus and soy protein isolate loaded with mupirocin. Sci Rep. 2024;14:26397.
27. Chao PC, Li Y, Chang CH, Shieh JP, Cheng JT, Cheng KC. Investigation of insulin resistance in the popularly used four rat models of type-2 diabetes. Biomed Pharmacother. 2018;101:155–61.
28. Wei Q, Su J, Meng S, Wang Y, Ma K, Li B, Chu Z, Huang Q, Hu W, Wang Z, et al. MiR-17-5p-engineered sEVs encapsulated in GelMA hydrogel facilitated diabetic wound healing by targeting PTEN and p21. Adv Sci (Weinh). 2024;11:e2307761.
29. Habiballa L, Salmonowicz H, Passos JF. Mitochondria and cellular senescence: implications for musculoskeletal ageing. Free Radic Biol Med. 2019;132:3–10.
30. Yannas IV, Lee E, Orgill DP, Skrabut EM, Murphy GF. Synthesis and characterization of a model extracellular matrix that induces partial regeneration of adult mammalian skin. Proc Natl Acad Sci U S A. 1989;86:933–7.
31. Seliktar D. Designing cell-compatible hydrogels for biomedical applications. Science. 2012;336:1124–8.
32. Ramsey DJ, Kwan JT, Sharma A. Keeping an eye on the diabetic foot: the connection between diabetic eye disease and wound healing in the lower extremity. World J Diabetes. 2022;13:1035–48.
33. Xiao X, Xu M, Yu H, Wang L, Li X, Rak J, Wang S, Zhao RC. Mesenchymal stem cell-derived small extracellular vesicles mitigate oxidative stress-induced senescence in endothelial cells via regulation of miR-146a/Src. Signal Transduct Target Ther. 2021;6:354.
34. Guo Q, Jin Y, Chen X, Ye X, Shen X, Lin M, Zeng C, Zhou T, Zhang J. NF-κB in biology and targeted therapy: new insights and translational implications. Signal Transduct Target Ther. 2024;9:53.
35. Xiao S, Zhao T, Wang J, Wang C, Du J, Ying L, Lin J, Zhang C, Hu W, Wang L, Xu K. Gelatin methacrylate (GelMA)-Based hydrogels for cell transplantation: an effective strategy for tissue engineering. Stem Cell Rev Rep. 2019;15:664–79.
36. Bitar MS. Diabetes impairs angiogenesis and induces endothelial cell senescence by Up-Regulating Thrombospondin-CD47-Dependent signaling. Int J Mol Sci. 2019;20.
37. Gan L, Liu D, Liu J, Chen E, Chen C, Liu L, Hu H, Guan X, Ma W, Zhang Y, et al. CD38 deficiency alleviates Ang II-induced vascular remodeling by inhibiting small extracellular vesicle-mediated vascular smooth muscle cell senescence in mice. Signal Transduct Target Ther. 2021;6:223.
38. Liu J, Guo B, Liu Q, Zhu G, Wang Y, Wang N, Yang Y, Fu S. Cellular Senescence: A Bridge Between Diabetes and Microangiopathy. Biomolecules. 2024;14.
39. Salminen A, Kaarniranta K. NF-kappaB signaling in the aging process. J Clin Immunol. 2009;29:397–405.
40. Tian S, Mei J, Zhang L, Wang S, Yuan Y, Li J, Liu H, Zhu W, Xu D. Multifunctional hydrogel microneedle patches modulating Oxi-inflamm-aging for diabetic wound healing. Small. 2024;20:e2407340.
41. Manning BD, Toker A. AKT/PKB signaling: navigating the network. Cell. 2017;169:381–405.
42. Wang Y, Wang L, Wen X, Hao D, Zhang N, He G, Jiang X. NF-κB signaling in skin aging. Mech Ageing Dev. 2019;184:111160.
43. Chen H, Tu M, Liu S, Wen Y, Chen L. Dendrobine alleviates cellular senescence and osteoarthritis via the ROS/NF-κB Axis. Int J Mol Sci. 2023;24.
44. Gonzalez AC, Costa TF, Andrade ZA, Medrado AR. Wound healing - A literature review. Bras Dermatol. 2016;91:614–20.
45. Kazemi N, Javad MM, Kaviani Y, Al-Musawi MH, Varshosaz J, Soleymani EBS, Tavakoli M, Alizadeh M, Sharifianjazi F, Salehi S, et al. Core-shell nanofibers containing L-arginine stimulates angiogenesis and full thickness dermal wound repair. Int J Pharm. 2024;653:123931.
46. Firuzeh M, Labbaf S, Enayati MH, Dinari M, Mirhaj M. Enhanced wound healing with a bilayered multifunctional quaternized chitosan-dextran-curcumin construct. Carbohydr Polym. 2025;352:123195.
47. Galiano RD, Tepper OM, Pelo CR, Bhatt KA, Callaghan M, Bastidas N, Bunting S, Steinmetz HG, Gurtner GC. Topical vascular endothelial growth factor accelerates diabetic wound healing through increased angiogenesis and by mobilizing and recruiting bone marrow-derived cells. Am J Pathol. 2004;164:1935–47.
48. Eming SA, Krieg T, Davidson JM. Inflammation in wound repair: molecular and cellular mechanisms. J Invest Dermatol. 2007;127:514–25.
49. Okonkwo UA, DiPietro LA. Diabetes and wound angiogenesis. Int J Mol Sci 2017, 18.
50. Sawada N, Jiang A, Takizawa F, Safdar A, Manika A, Tesmenitsky Y, Kang KT, Bischoff J, Kalwa H, Sartoretto JL, et al. Endothelial PGC-1α mediates vascular dysfunction in diabetes. Cell Metab. 2014;19:246–58.
51. Zhang L, Pitcher LE, Yousefzadeh MJ, Niedernhofer LJ, Robbins PD, Zhu Y. Cellular senescence: a key therapeutic target in aging and diseases. J Clin Invest. 2022;132.
52. Tavakoli M, Al-Musawi MH, Kalali A, Shekarchizadeh A, Kaviani Y, Mansouri A, Nasiri-Harchegani S, Kharazi AZ, Sharifianjazi F, Sattar M, et al. Platelet rich fibrin and simvastatin-loaded pectin-based 3D printed-electrospun bilayer scaffold for skin tissue regeneration. Int J Biol Macromol. 2024;265:130954.
53. Koupai AA, Varshosaz J, Dobakhti F, Shekarchizadeh F, Al-Musawi MH, Kamil MM, Turki SH, Valizadeh H, Sharifianjazi F, Tavakoli M, Mirhaj M. Vanillin and IGF1-loaded dual-layer multifunctional wound dressing with micro-nanofibrous structure for full-thickness wound healing acceleration. Int J Pharm. 2025;671:125231.
54. Pakyari M, Farrokhi A, Maharlooei MK, Ghahary A. Critical role of transforming growth factor Beta in different phases of wound healing. Adv Wound Care (New Rochelle). 2013;2:215–24.
55. Ji Y, Zhang A, Chen X, Che X, Zhou K, Wang Z. Sodium humate accelerates cutaneous wound healing by activating TGF-β/Smads signaling pathway in rats. Acta Pharm Sin B. 2016;6:132–40.
56. Almajidi YQ, Muslim RK, Issa AA, Al-Musawi MH, Shahriari-Khalaji M, Mirhaj M. Three-dimensional printed polyelectrolyte construct containing mupirocin-loaded quaternized Chitosan nanoparticles for skin repair. Int J Biol Macromol. 2024;280:136214.
57. Shahriari-Khalaji M, Sattar M, Wei H, Al-Musawi MH, Ibrahim YY, Hasan TS, Yang S, Tavakoli M, Mirhaj M. Physicochemically Cross-linked injectable hydrogel: an adhesive skin substitute for burned wound therapy. ACS Appl Bio Mater. 2025.

Publisher's note